



Krypton-derivatization highlights O₂-channeling in a four-electron reducing oxidase†

 Sylvain Engilberge,^{id} ‡^a Tristan Wagner,^{id} ‡^b Philippe Carpentier,^{id} ^{cd}
 Eric Girard^{id} *^e and Seigo Shima^{id} *^f

 Cite this: *Chem. Commun.*, 2020, 56, 10863

 Received 1st July 2020,
 Accepted 3rd August 2020

DOI: 10.1039/d0cc04557h

rsc.li/chemcomm

F₄₂₀H₂-oxidase (FprA) catalyses the four-electron reduction of O₂ to 2H₂O using the reduced form of F₄₂₀ as electron donor. The hydrophobic O₂-channel detected by Kr-derivatization and the concerted movement of a gating loop could contribute to prevent unwanted side-reaction between the catalytic intermediates and solvents, therefore preventing reactive oxygen species formation.

Electrochemical reactions require electro catalysts functioning as a cathode and anode.¹ Metal-containing redox-enzymes are considered as blueprints to design mimic complexes for the development of efficient electro catalysts. For example, some oxidases (e.g. laccase) harbour cathode catalyst property by using O₂ as an electron acceptor and the chemical compounds mimicking their active-site are used as electrocatalysts.² For future application of bio-inspired electrochemical processes, we need to learn more from the chemical reaction, structure and function of different groups of O₂-reducing enzymes. Flavodiiron proteins (FDPs) belong to an enzyme family harbouring a di-nuclear iron centre and flavin mononucleotide (FMN). FDPs catalyse four-electron reduction of O₂ to form water.^{3,4} The active site of FDPs represents an excellent template to design O₂ reducing catalysts because of its affinity towards O₂, high-turnover and specific reaction path avoiding

reactive oxygen species formation. The latter would damage the catalysts in the electrochemical systems.

FprA has been found in many anaerobic organisms (Fig. S1, ESI†), initially in *Desulfovibrio gigas*⁵ and later also in methanogens^{6,7} and clostridia.^{8,9} It has even been identified in the parasite *Giardia intestinalis*.¹⁰ Structural studies have been performed on these FprAs to understand the physiological electron donor for the reaction and highlight high fold similarity between homologous enzymes (Fig. S2, ESI†).^{7,9–12} In methanogenic archaea, the electron donor of the reaction (Fig. 1a) is reduced F₄₂₀ (F₄₂₀H₂).⁶ F₄₂₀ is a deazaflavin derivative, which functions as electron carrier. Affinity of FprA against O₂ is 2 μM,⁶ which is lower than those of laccases (K_m > 20 μM).¹³

Crystal structure of FprA from *Methanothermobacter marburgensis* (mFprA) was solved in three states; active reduced state, active oxidized state and inactive oxidized state at the resolutions

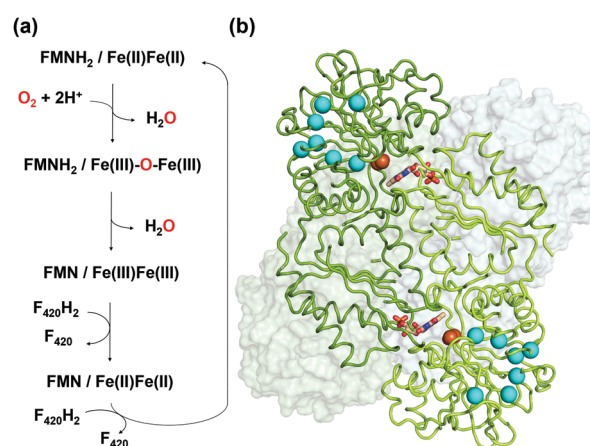


Fig. 1 (a) Reaction scheme of FprA. The tFprA_{anox} and tFprA_{oxo} forms correspond to the redox state at Fe(II)Fe(II) and Fe(III)–O–Fe(III), respectively. (b) Quaternary structure of tFprA organized as a dimer of homodimer. A first homodimer is displayed in the back as white surface. The second one in front (green ribbon) highlights the di-iron centre as orange spheres and FMN in sticks. Kr atoms in the tFprA_{O₂-Kr} structure after derivatization with 125 bars of krypton are depicted in cyan spheres.

^a Paul Scherrer Institut, Forschungsstrasse 111, 5232 Villigen PSI, Switzerland

^b Microbial Metabolism Group, Max-Planck-Institut für Marine Mikrobiologie, Celsiusstraße 1, 28359, Bremen, Germany

^c Institut de Recherche Interdisciplinaire de Grenoble (IRIG), Laboratoire Chimie et Biologie des Métaux (LCBM), Université Grenoble Alpes, CNRS, CEA, Grenoble, France

^d European Synchrotron Radiation Facility (ESRF), Grenoble, France

^e Univ. Grenoble Alpes, CEA, CNRS, IBS, F-38000 Grenoble, France.

E-mail: eric.girard@ibs.fr

^f Microbial Protein Structure Group, Max Planck Institute for Terrestrial Microbiology, Karl-von-Frisch Straße 10, 35043 Marburg, Germany.

E-mail: shima@mpi-marburg.mpg.de

† Electronic supplementary information (ESI) available: Methods, Fig. S1–S8, Tables S1 and S2 and references. See DOI: 10.1039/d0cc04557h

‡ Both authors contributed equally to this work.



Romão and co-workers.²⁰ To characterize experimentally this possible gas channel, we produced Kr-derivatives of oxidized tFprA by flash cooling crystals under gas pressure and collected datasets below and above the Kr K-edge (SI Method and Table S1, ESI†). Anomalous signal coming unambiguously from Kr atoms have been detected in an anomalous Fourier map at similar positions in each of the eight monomers constituting the asymmetric unit (Fig. S8, ESI†). Up to six Kr were localized in a hydrophobic channel (Fig. 1b and 2b, c, Fig. S8, ESI†). The narrow channel is ~ 30 Å long and has an average radius of 1.2 Å, which is in accordance with the size of O₂ molecule. The channel is built at the conserved interface (Fig. S2, ESI†) between the anti-parallel β -sheets $\beta 13\beta 14\beta 15$ and the α -helices 6 and 7. It starts from the surface and ends at the di-iron site. The hydrophobic channel simulated by the CAVER software in tFprA_{anox} structure (Fig. 2c and Fig. S3, ESI†) perfectly coincides with the Kr positions. Comparison between tFprA_{anox} and tFprA_{oxo-Kr} does not indicate any channel distortion or size modification upon pressurisation and Kr binding.

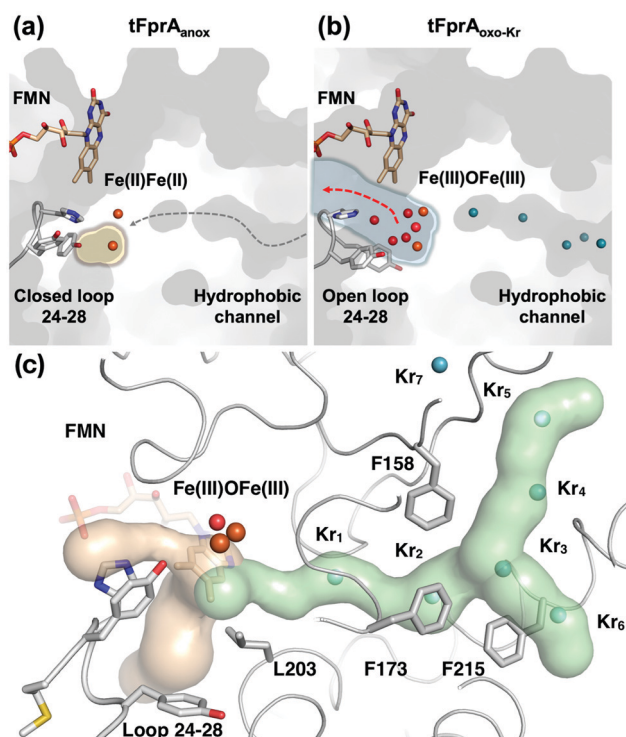


Fig. 2 Structure of the active site and a hydrophobic O₂-channel. (a) tFprA_{anox} structure, in which the loop 24–28 is fixed as a closed conformation and isolates the catalytic cavity highlighted by a yellow halo. The predicted O₂ pathway is indicated with a gray dashed arrow. (b) tFprA_{oxo-Kr} structure after derivatization with 125 bars of krypton, in which the loop 24–28 is flexible compared to tFprA_{anox}. The water channel is depicted by light blue halo and a red arrow indicates solvent exchange. Kr are depicted as cyan balls. (c) tFprA channels identified by CAVER in tFprA_{anox} structure. Hydrophobic part of the channel is depicted in light green. Kr atoms from tFprA_{oxo-Kr} structures are superimposed as cyan spheres. Hydrophilic part of the channel involved in water release after O₂ reduction is depicted in light orange. Di-iron centre is highlighted as orange spheres, FMN and the loop 24–28 in sticks. Y28 in tFprA_{anox} exists as a double conformation and only the one at highest occupancy (70%) is displayed.

Kr_{4,5} and Kr₆ highlight two possible entrances for the O₂ (Fig. 1b, 2c and Fig. S8, ESI†). Interestingly, a modulation in the Kr atoms occupancies along the channel is observed. Two main Kr atoms Kr₂ and Kr₃ are trapped in a high hydrophobic/rigid part of the channel formed by three phenylalanine's side chains (F158, F173, F215) (Fig. 2c). These two Kr atoms present high occupancies (0.75) compared to the four other ones (Kr₁, Kr₄, Kr₅ and Kr₆). This might suggest a lower affinity for Kr and therefore also for O₂ in the outer part of the tunnel (Kr_{4,5} and Kr₆) and at that close to the iron centre (Kr₁) in the oxidized state. The high Kr affinity part of the tunnel also probably acts as a “retention cavity” and could play a role in the kinetics of O₂ transport. Similar variation in Kr-binding were also observed in other O₂ hydrophobic tunnels.²¹ The Kr₁ atom (occupancy 0.1) observed near the di-iron site points out the final destination of O₂ from the gas channel, which could be the O₂-binding site, where O₂ is in interaction with the di-iron site centre. Kr₇ atom is located outside of the channel in a hydrophobic pocket. The hydrophobic residues lining the channel are very well conserved in methanogens and could be extended to other dinuclear oxidases such as those from *Giardia intestinalis*¹⁰ and *Moorella thermoactica*⁹ (Fig. S1 and S2, ESI†). CAVER simulation argues for a common O₂ route in all structural homologues available (Fig. S3, ESI†). This finding highlights the universal needs of such hydrophobic channel to specifically react with O₂ or NO. CAVER analysis also identified a hydrophilic channel in the oxidized state, likely the channel involved in water release. This second channel (Fig. 2) starts from the di-iron site at the end of the O₂ channel, includes the loop 24–28 and finishes in the large hydrophilic cavity formed by the FprA tetrameric interface.

The FprA reaction is performed by a ping-pong mechanism using two molecules of F₄₂₀H₂. When the di-iron centre and FMN are completely reduced to Fe(II)Fe(II) and FMNH₂, the loop 24–28 would lock the entrance of the water channel. In tFprA_{anox}, Y28 might contribute to bridge the hydrophilic gap and prevent unwanted side reactions by moving close to L203, which is one of the last amino acid of the hydrophobic channel (Fig. 2c). The channel ends-up in front of the empty di-iron site (tFprA_{anox}), where O₂ could bind, as previously predicted by the analysis of mFprA. The first two-electron reduction is performed by the Fe(II)Fe(II). O₂ is first bound to the dinuclear Fe site, which forms transient bridged Fe(III) peroxo intermediate^{7,22,23} and then form a water molecule with the first oxygen atom, while the second one is trapped at the di-iron site to form an oxo-bridge Fe(III)–O–Fe(III). Protons required for the water-forming reactions are supplied from the histidine side-chains (H84–H152 and H89–H234), which coordinate the irons. The formed water molecule is repelled from the hydrophobic region when H26 and Y28 become more flexible, and open the hydrophilic channel (Fig. 3). After removal of the first water molecule from the active site pocket, the loop 24–28 is restabilized, probably upon the reduction event by FMNH₂. In the closed structure, reduction of oxygen bound to the dinuclear iron site is performed in the absence of water molecule. After that, the water channel opens again and the





Fig. 3 Contribution of the hydrophobic O₂-channel, loop 24–28 and water channel in the catalytic mechanism. The hydrophobic O₂-channel (gray) and hydrophilic water-channels (light blue) are indicated. In the reduced state, the loop is closed and fixed (green and gray dashed line). After the first water is produced, the switch loop is still closed but becomes flexible (orange), where the water is released to bulk solvent.

water molecule is released. The driving-force able to guide the closure and opening of the 24–28 loop to prevent or allow solvent accessibility could be the FMN state or even the F₄₂₀H₂ binding that could lead to a local rearrangement. For instance, the isoalloxazine group is in van der Waals contact with the loop 24–28 (3.4–4.2 Å) and could contribute to stabilise or destabilise the loop depending on its state.

In conclusion, previous biochemical studies indicated that FprA catalyses reduction of O₂ with four electrons supplied by two molecules of F₄₂₀H₂. The reaction avoids the generation of reactive oxygen species, hydrogen peroxide and superoxide anion. Seedorf *et al.* proposed a catalytic mechanism involving a Fe(III)–O–Fe(III), which does not produce reactive oxygen species as an intermediate. However, the mechanism did not explain how to supply O₂ into the active site while stopping water intrusion. The shape and position of the hydrophobic channel allowed us to draw a reaction scheme taking into account a water repulsion system to avoid unwanted reaction. Such reaction scheme would require a gating system by surrounding loops coordinating the reactivity of the catalytic chamber, which is a conserved system retained by life in numerous organisms dealing with oxidative stress.

The authors acknowledge funding by Agence Nationale de la Recherche (ANR) grant (program Ln23 ANR-13-BS07-0007-01), Swiss National Science Foundation grant (200021-182369), Deutsche Forschungsgemeinschaft, (SH 87/1-1) and the Max Planck Society. This work used the platforms of the Grenoble Instruct center (ISBG; UMS 3518 CNRS-CEA-UJF-EMBL) with support from FRISBI (ANR-10-INSB-05-02) and GRAL (ANR-10-LABX-49-01) within the Grenoble Partnership for Structural Biology (PSB). We thank ESRF synchrotron (id29 beamline) and SOLEIL synchrotron (PXII beamline) for beam time allocation and the respective beamline staffs for assistance with data collection.

We also acknowledge access to the ESRF MX high-pressure laboratory (HPMX). IBS acknowledges integration into the Interdisciplinary Research Institute of Grenoble (IRIG, CEA).

Open Access funding provided by the Max Planck Society.

Conflicts of interest

There are no conflicts to declare.

Notes and references

- 1 A. Kulkarni, S. Siahrostami, A. Patel and J. K. Nørskov, *Chem. Rev.*, 2018, **118**, 2302–2312.
- 2 C. F. Blanford, C. E. Foster, R. S. Heath and F. A. Armstrong, *Faraday Discuss.*, 2009, **140**, 319–335.
- 3 F. Folgosa, M. C. Martins and M. Teixeira, *FEMS Microbiol. Lett.*, 2018, **365**, fnx267.
- 4 K. A. Brown, Z. J. Guo, M. Tokmina-Lukaszewska, L. W. Scott, C. E. Lubner, S. Smolinski, D. W. Mulder, B. Bothner and P. W. King, *Sustainable Energy Fuels*, 2019, **3**, 3191–3200.
- 5 L. Chen, M. Y. Liu, J. Legall, P. Fareleira, H. Santos and A. V. Xavier, *Biochem. Biophys. Res. Commun.*, 1993, **193**, 100–105.
- 6 H. Seedorf, A. Dreisbach, R. Hedderich, S. Shima and R. K. Thauer, *Arch. Microbiol.*, 2004, **182**, 126–137.
- 7 H. Seedorf, C. H. Hagemeyer, S. Shima, R. K. Thauer, E. Warkentin and U. Ermler, *FEBS J.*, 2007, **274**, 1588–1599.
- 8 A. Das, R. Silaghi-Dumitrescu, L. G. Ljungdahl and D. M. Kurtz Jr, *J. Bacteriol.*, 2005, **187**, 2020–2029.
- 9 R. Silaghi-Dumitrescu, D. M. Kurtz Jr, L. G. Ljungdahl and W. N. Lanzilotta, *Biochemistry*, 2005, **44**, 6492–6501.
- 10 A. Di Matteo, F. M. Scandurra, F. Testa, E. Forte, P. Sarti, M. Brunori and A. Giuffrè, *J. Biol. Chem.*, 2008, **283**, 4061–4068.
- 11 H. Fang, J. D. Caranto, R. Mendoza, A. B. Taylor, P. J. Hart and D. M. Kurtz Jr, *J. Biol. Inorg. Chem.*, 2012, **17**, 1231–1239.
- 12 C. Frazão, G. Silva, C. M. Gomes, P. Matias, R. Coelho, L. Siker, S. Macedo, M. Y. Liu, S. Oliveira, M. Teixeira, A. V. Xavier, C. Rodrigues-Pousada, M. A. Carrondo and J. Le Gall, *Nat. Struct. Biol.*, 2000, **7**, 1041–1045.
- 13 F. Xu, *Appl. Biochem. Biotechnol.*, 2001, **95**, 125–133.
- 14 B. L. Victor, A. M. Baptista and C. M. Soares, *J. Biol. Inorg. Chem.*, 2009, **14**, 853–862.
- 15 N. Colloc'h, P. Carpentier, L. C. Montemiglio, B. Vallone and T. Prange, *Biophys. J.*, 2017, **113**, 2199–2206.
- 16 B. Lafumat, C. Mueller-Dieckmann, G. Leonard, N. Colloc'h, T. Prange, T. Giraud, F. Dobias, A. Royant, P. van der Linden and P. Carpentier, *J. Appl. Crystallogr.*, 2016, **49**, 1478–1487.
- 17 V. M. Luna, Y. Chen, J. A. Fee and C. D. Stout, *Biochemistry*, 2008, **47**, 4657–4665.
- 18 J. P. Kallio, J. Rouvinen, K. Kruus and N. Hakulinen, *Biochemistry*, 2011, **50**, 4396–4398.
- 19 S. Engilberge, T. Wagner, G. Santoni, C. Breyton, S. Shima, B. Franzetti, F. Riobé, O. Maury and E. Girard, *J. Appl. Crystallogr.*, 2019, **52**, 722–731.
- 20 C. V. Romão, J. B. Vicente, P. T. Borges, B. L. Victor, P. Lamosa, E. Silva, L. Pereira, T. M. Bandejas, C. M. Soares, M. A. Carrondo, D. Turner, M. Teixeira and C. Frazão, *J. Mol. Biol.*, 2016, **428**, 4686–4707.
- 21 J. Kalms, A. Schmidt, S. Frielingsdorf, P. van der Linden, D. von Stetten, O. Lenz, P. Carpentier and P. Scheerer, *Angew. Chem., Int. Ed.*, 2016, **55**, 5586–5590.
- 22 M. Costas, C. W. Cady, S. V. Kryatov, M. Ray, M. J. Ryan, E. V. Rybak-Akimova and L. Que Jr, *Inorg. Chem.*, 2003, **42**, 7519–7530.
- 23 S. V. Kryatov, E. V. Rybak-Akimova, V. L. MacMurdo and L. Que Jr, *Inorg. Chem.*, 2001, **40**, 2220–2228.

